GEOPHYSICS, VOL. 66, NO. 1 (JANUARY-FEBRUARY 2001); P. 294–307, 13 FIGS.

Application of the perfectly matched absorbing layer model to the linear elastodynamic problem in anisotropic heterogeneous media

Francis Collino and Chrysoula Tsogka*

ABSTRACT

We present and analyze a perfectly matched, absorbing layer model for the velocity-stress formulation of elastodynamics. The principal idea of this method consists of introducing an absorbing layer in which we decompose each component of the unknown into two auxiliary components: a component orthogonal to the boundary and a component parallel to it. A system of equations governing these new unknowns then is constructed. A damping term finally is introduced for the component orthogonal to the boundary. This layer model has the property of generating no reflection at the interface between the free medium and the artificial absorbing medium. In practice, both the boundary condition introduced at the outer boundary of the layer and the dispersion resulting from the numerical scheme produce a small reflection which can be controlled even with very thin layers. As we will show with several experiments, this model gives very satisfactory results; namely, the reflection coefficient, even in the case of heterogeneous, anisotropic media, is about 1% for a layer thickness of five space discretization steps.

INTRODUCTION

The simulation of waves by finite-difference or finite-element methods in unbounded domains requires a special treatment for the boundaries of the necessarily truncated computational domain. Two solutions have been proposed for this purpose: absorbing boundary conditions (ABCs) and absorbing layers. ABCs were introduced by B. Engquist and A. Majda (1977) for the acoustic wave equation. They consist of introducing some suitable local boundary conditions that simulate the outgoing nature of the waves impinging on the borders. This method works particularly well for absorbing waves nearly normally incident to the artificial boundaries. For waves traveling obliquely to the boundary, higher-order ABCs must be used to achieve acceptable accuracy (Hagstrom, 1997).

For elastic waves, the situation is more complex. First, the transparent condition, i.e., the exact condition relating normal stress and displacement on a line for outgoing waves, is no longer a scalar but a matrix integro-differential relation. Its approximation by partial differential equations, which is the usual way to construct ABCs, leads to a very complex system of equations, especially for higher-order methods. The stability of the coupled problem composed of the elastodynamic system completed by these artificial conditions is then very difficult to analyze, and the situation is even more intricate when discretization is considered (Chalindar, 1987). To overcome these difficulties, Higdon (1991, 1992) proposed combining several first-order boundary conditions designed for the wave equation, each of them being associated with either the pressure-wave velocity or the shear-wave velocity. These conditions are theoretically stable (Higdon, 1990), relatively easy to implement, and efficient for waves traveling in a direction close to the normal of the artificial boundaries. They also can be adapted to the case of surface waves (Sochacki et al., 1987). However, for other directions of propagation, important spurious reflections may occur. Some authors, Peng and Toksoz (1995), for instance, have proposed optimizing the coefficients of Higdon's method to make these reflections decrease. However, numerical experiments still show relatively strong spurious reflections in some situations and stability problems when higher-order numerical schemes are used (Simone and Hestholm, 1998).

Layer models are an alternative to ABCs. The idea is to surround the domain of interest by some artificial absorbing layers in which waves are trapped and attenuated. For elastic waves, several models have been proposed. For instance, Sochacki et al. (1987) suggest adding inside the layers some attenuation term, proportional to the first time derivative of the displacement to the elastodynamic equations. This technique, inspired by physics, is quite delicate in practice. The main difficulty is that when entering the layers, the wave "sees" the change in impedance of the medium and then is reflected

Manuscript received by the Editor August 26, 1998; revised manuscript received July 28, 1999.
*INRIA, Domaine de Voluceau, BP 105, 78153 Le Chesnay Cedex, France. E-mail: Chrysoula.Tsogka@inria.fr.

Reprinted from Geophysics, 66, 294–307. © 2001 Society of Exploration Geophysicists

artificially into the domain of interest. The use of smooth and not too high attenuation profiles allows us to weaken the difficulty but requires the use of thick layers (Israeli and Orszag, 1981).

In this paper, we propose adapting a layer technique introduced by Bérenger (1994) for Maxwell's equations and that is now the most widely used method for the simulation of electromagnetic waves in nonbounded domains (Bérenger, 1996, 1997; Zhao and Cangellaris, 1996; Teixeira and Chew, 1998; Turkel and Yefet, 1998). This technique consists of designing an absorbing layer called a perfectly matched layer (PML) that possesses the property of generating no reflection at the interface between the free medium and the artificial absorbing medium. This property allows us to use a very high damping parameter inside the layer and consequently a small layer width while achieving a quasi-perfect absorption of the waves. To our knowledge, this method previously has been used only once for elastic waves simulation. In Hastings et al. (1996), the authors propose the use of PML for the compressional and shear potentials formulation. In our paper, the PMLs are incorporated into the stress-velocity formulation.

The present paper is organized as follows. In section two, we construct the PML model in the general case of an evolution problem. It is based on an interpretation of the PML model of Bérenger (1994) as a change of variable in the complex plane [compare Rappaport (1995), Collino (1996)]. In section three, we apply the previous model to the velocity-stress formulation for elastodynamics and we study the properties of the continuous PML model via a plane-wave analysis. To show the generality of the PML model, two numerical schemes are presented, in section four. The first is the classical Virieux finite-differences scheme (Virirux, 1986), and the second is a mixed finite-element scheme (Bécache et al., 1997) which allows us to consider anisotropic media as well. Finally, in section five, we present several numerical results which show the efficiency of this model even in the case of heterogeneous, anisotropic elastic media and their superiority when compared with the classical ABC method.

PML MODEL FOR A GENERAL EVOLUTION PROBLEM

We will present in this section the basic principles of the PML model in the general case of an evolution problem. This will allow us to generalize it to other models of wave propagation. Consider a general evolution problem of the following form

$$\begin{aligned} (a)\quad & \partial_t v - A\partial_x v - B\partial_y v = 0, \\ (b)\quad & v(t=0) = v_0, \end{aligned} \tag{1}$$

where, in the general case, v is a m-vector, A is an $m \times m$ matrix, $x \in \mathbb{R}$, and $y \in \mathbb{R}^{n-1}$. To simplify the presentation, in what follows, we consider the scalar case with $m = 1$ and $n = 2$. Moreover, we assume that the initial condition v_0 is zero on the right half-space. We would like to replace problem (1) by an equivalent one posed in the left half-space. The basic principle of the PML model is to couple the equation in the left half-space with an equation in the right half-space such that there is *no reflection* at the interface, and that the wave *decreases exponentially* inside the right half-space. Thus, we first introduce the following system,

$$\begin{aligned} \partial_t v^{\parallel} - B\partial_y v = 0, \\ \partial_t v^{\perp} - A\partial_x v = 0, \end{aligned} \tag{2}$$

with $v = v^{\parallel} + v^{\perp}$, and where superscript $\parallel$ means that we keep only the derivative parallel to the interface, i.e., the y-derivative (superscript $\perp$ means that only the x-derivative is considered). It is easy to see that system (2) implies (1)-(a). Second, we introduce a function $d(x)$, zero on the left half-space and positive on the right-half space. This function will play the role of the damping factor. We define now a new wave, u, solution of the following system,

$$\begin{aligned} \partial_t u^{\perp} + d(x)u^{\perp} - A\partial_x u = 0, \\ \partial_t u^{\parallel} - B\partial_y u = 0, \\ u(t=0) = v_0, \end{aligned} \tag{3}$$

with $u = u^{\parallel} + u^{\perp}$. It is easy to see that u satisfies the same system of equations as v in the left half-space. If we look for time-harmonic solutions of system (1) with angular frequency ω, we get

$$i\omega\hat{v} - A\partial_x\hat{v} - B\partial_y\hat{v} = 0.$$

In the same way, the time-harmonic solutions of system (3) satisfy

$$\begin{aligned} (i\omega + d(x))\hat{u}^{\perp} - A\partial_x\hat{u} = 0, \\ i\omega\hat{u}^{\parallel} - B\partial_y\hat{u} = 0, \end{aligned}$$

with $\hat{u} = \hat{u}^{\parallel} + \hat{u}^{\perp}$ or, equivalently,

$$\begin{aligned} i\omega\hat{u}^{\perp} - \frac{i\omega}{i\omega + d(x)} A\partial_x\hat{u} = 0, \\ i\omega\hat{u}^{\parallel} - B\partial_y\hat{u} = 0, \end{aligned}$$

with $\hat{u} = \hat{u}^{\parallel} + \hat{u}^{\perp}$. We can remark now that the PML model consists of the simple substitution

$$\partial_x \to \partial_{\tilde{x}} = \frac{i\omega}{i\omega + d(x)}\partial_x,$$

which implies the complex change of variables

$$\tilde{x}(x) = x - \frac{i}{\omega}\int_0^x d(s)\,ds.$$

We now can study the properties of this model using a plane-wave analysis. We seek particular solutions of system (1) in the following form,

$$\begin{aligned} v &= v_0 \exp[-i(k_x x + k_y y - \omega t)], \\ k &= (k_x, k_y) \in \mathbb{R} \times \mathbb{R},\ \omega \in \mathbb{R}. \end{aligned} \tag{4}$$

Formula (4) is a plane wave propagating in the direction k with the phase velocity $\omega/|k|$. To be a solution to problem (1), v has to satisfy the following relation:

$$i v_0\omega - iA v_0 k_x - iB v_0 k_y = 0. \tag{5}$$

In the same way, we seek particular solutions of system (3) in the following form

$$\begin{aligned} u^{\parallel} &= a^{\parallel} \exp[-i(k_x\tilde{x}(x) + k_y y - \omega t)], \\ u^{\perp} &= a^{\perp} \exp[-i(k_x\tilde{x}(x) + k_y y - \omega t)], \\ u &= u^{\parallel} + u^{\perp}. \end{aligned}$$

To be a solution to problem (3), $u^{\parallel}$ and $u^{\perp}$ have to satisfy the following relations:

$$\begin{aligned} ia^{\parallel}\omega - iB(a^{\perp}+a^{\parallel})k_y = 0,\\ (i\omega + d(x))a^{\perp} - i\left(1-\frac{id(x)}{\omega}\right)A(a^{\perp}+a^{\parallel})k_x = 0 \end{aligned} \tag{6}$$

or, equivalently,

$$\begin{aligned} ia^{\parallel}\omega - iB(a^{\perp}+a^{\parallel})k_y = 0,\\ ia^{\perp}\omega - iA(a^{\perp}+a^{\parallel})k_x = 0. \end{aligned} \tag{7}$$

Adding the two equalities of (7) gives

$$i(a^{\perp}+a^{\parallel})\omega - iA(a^{\perp}+a^{\parallel})k_x - iB(a^{\perp}+a^{\parallel})k_y = 0. \tag{8}$$

We can remark now that if we chose $a^{\perp}$ and $a^{\parallel}$ such that

$$a^{\perp}+a^{\parallel} = v_0,$$

equation (8) becomes the same as (5). Moreover, from (7) we get

$$a^{\parallel} = Bv_0\frac{k_y}{\omega}, \qquad a^{\perp} = Av_0\frac{k_x}{\omega}, \tag{9}$$

which gives the plane-wave solution of (3). We then have the following property: The plane wave solution of system (3) can be written in the form

$$u = v_0\exp[-i(k_x x + k_y y - \omega t)]\exp\left[-\frac{k_x}{\omega}\int_0^x d(s)\,ds\right],$$

and satisfies:

1) $u \equiv v$ in the left half-space, $x \le 0$, which means that we have no reflection at the interface; the layer model is matched perfectly.
2) u is damped in the right half-space,
3) the damping coefficient in the absorbing half-space is

$$\alpha_d = \frac{\|u(x)\|}{\|v(x)\|} = \exp\left[-\frac{k_x}{\omega}\int_0^x d(s)\,ds\right]. \tag{10}$$

Relation (10) implies that the waves decrease exponentially in the absorbing half-space. The damping coefficient (α_d) depends on the direction of propagation of the wave. More precisely, α_d decreases very quickly for a wave propagating normally to the interface and decreases more and more slowly as the direction of propagation approaches the parallel to the interface.

PML MODEL FOR ELASTODYNAMICS

In this section, we present the PML model for the continuous elastodynamic problem. As we have seen in section two, we know how to construct a PML model for an evolution problem of the form (1). Thus, to apply the technique described in the previous section to elastodynamics, we need to write the elastodynamic problem in the form of system (1). This can be done easily once we consider the mixed velocity-stress formulation for elastodynamics.

The elastodynamic problem

We consider the 2-D elastodynamic problem written as a first-order hyperbolic system, the so called velocity-stress system

$$\begin{aligned} \varrho\,\partial_t v - \mathbf{div}\,\sigma = 0,\\ A\partial_t\sigma - \varepsilon(v) = 0, \end{aligned} \tag{11}$$

together with initial conditions. We suppose, as in the previous section, that the initial condition is supported in the left half-space. In equation (11), $v = (v_x, v_y)$ denotes the velocity, σ the stress tensor, and $\varrho = \varrho(x)$ the density. If $u = (u_x, u_y)$ is the displacement, then $v = \partial_t u$. We denote $\varepsilon(u)$ the linearized strain tensor, i.e.,

$$\varepsilon_{ij}(u) = \frac{1}{2}(\partial_j u_i + \partial_i u_j).$$

The stress tensor is related to the strain tensor by the generalized Hooke's law

$$\sigma = \sigma(u)(x,t) = C(x)\varepsilon(u)(x,t),$$

where stiffness $C(x)$ is a 4×4 positive tensor having the classical properties of symmetry (Auld, 1973). In system (11), we used the compliance tensor

$$A = A(x) = C^{-1}(x).$$

Finally, we identify the stress tensor σ with the following vector (still denoted by σ)

$$\sigma = [\sigma_1,\ \sigma_2,\ \sigma_3]^T,$$
$$\sigma_1 = \sigma_{xx}; \quad \sigma_2 = \sigma_{yy}; \quad \sigma_3 = \sigma_{xy}.$$

We can write (11) in the following matrix form

$$\begin{aligned} \varrho\,\partial_t v = D^{\parallel}\partial_y\sigma + D^{\perp}\partial_x\sigma \text{ in } \Omega,\\ A\partial_t\sigma = E^{\parallel}\partial_y v + E^{\perp}\partial_x v \text{ in } \Omega\,, \end{aligned}$$

with

$$D^{\parallel} = \begin{bmatrix} 0 & 0 & 1\\ 0 & 1 & 0 \end{bmatrix}, \quad D^{\perp} = \begin{bmatrix} 1 & 0 & 0\\ 0 & 0 & 1 \end{bmatrix},$$

$$E^{\parallel} = \begin{bmatrix} 0 & 0 & 1\\ 0 & 1 & 0 \end{bmatrix}^T, \quad E^{\perp} = \begin{bmatrix} 1 & 0 & 0\\ 0 & 0 & 1 \end{bmatrix}^T.$$

We can apply now the same technique as in section two, and we get the following system in the perfectly matched layer($x > 0$):

$$v = v^{\parallel} + v^{\perp}; \quad \sigma = \sigma^{\parallel} + \sigma^{\perp},$$
$$\varrho\,\partial_t v^{\parallel} = D^{\parallel}\partial_y\sigma; \quad A\partial_t\sigma^{\parallel} = E^{\parallel}\partial_y v,$$
$$\varrho\,\partial_t v^{\perp} + d(x)v^{\perp} = D^{\perp}\partial_x\sigma; \quad A\sigma^{\perp} = E^{\perp}\partial_x v,$$

where $d(x)$ denotes the damping factor. In a homogeneous, isotropic elastic medium, the matrix $C(x)$ depends on the Lamé coefficients (λ, μ) of the medium. In this case, the PML model

can be written in the following form:

$$
\begin{aligned}
v = v^{\parallel} + v^{\perp}; \quad \sigma = \sigma^{\parallel} + \sigma^{\perp},\\
\varrho(\partial_t + d(x))v_x^{\perp} = \partial_x \sigma_{xx}; \quad \varrho\partial_t v_x^{\parallel} = \partial_y \sigma_{xy},\\
\varrho(\partial_t + d(x))v_y^{\perp} = \partial_x \sigma_{xy}; \quad \varrho\partial_t v_y^{\parallel} = \partial_y \sigma_{yy},\\
(\partial_t + d(x))\sigma_{xx}^{\perp} = (\lambda + 2\mu)\partial_x v_x; \quad \partial_t \sigma_{xx}^{\parallel} = \lambda\partial_y v_y,\\
(\partial_t + d(x))\sigma_{yy}^{\perp} = \lambda\partial_x v_x; \quad \partial_t \sigma_{yy}^{\parallel} = (\lambda + 2\mu)\partial_y v_y,\\
(\partial_t + d(x))\sigma_{xy}^{\perp} = \mu\partial_x v_y; \quad \partial_t \sigma_{xy}^{\parallel} = \mu\partial_y v_x.
\end{aligned}
\tag{12}
$$

Plane-wave analysis

Infinite absorbing layer.—In the case of a homogeneous, isotropic elastic medium, following the same technique as in section two, we can show that the displacement plane waves, U_j, $j = p, s$, corresponding to solutions of system (11), can be written in the following form,

$$
\begin{aligned}
U_p &= A_p \mathbf{d}_p \exp\left[i\omega V_p\left(t - \frac{\cos(\theta)x + \sin(\theta)y}{V_p}\right)\right],\\
U_s &= A_s \mathbf{d}_s \exp\left[i\omega V_s\left(t - \frac{-\sin(\theta)x + \cos(\theta)y}{V_s}\right)\right],
\end{aligned}
\tag{13}
$$

where $V_p = \sqrt{(\lambda + 2\mu)/\varrho}$ is the pressure-wave velocity, $V_s = \sqrt{\mu/\varrho}$ is the shear-wave velocity, θ gives the direction of wave propagation, $\mathbf{d}_j$, $j = p, s$ defines the direction of particle motion, and A_j, $j = p, s$ is the amplitude of the wave. We can remark then that the displacement plane waves, $\tilde{U}_j$ (for $j = p, s$), solutions of system (12), can be written as

$$
\begin{aligned}
\tilde{U}_p &= A_p \mathbf{d}_p \exp\left[i\omega V_p\left(t - \frac{\cos(\theta)\tilde{x}_p + \sin(\theta)y}{V_p}\right)\right],\\
\tilde{U}_s &= A_s \mathbf{d}_s \exp\left[i\omega V_s\left(t - \frac{-\sin(\theta)\tilde{x}_s + \cos(\theta)y}{V_s}\right)\right],
\end{aligned}
\tag{14}
$$

where we simply substituted $\tilde{x}_j$, $j = p, s$ for x in (13), with $\tilde{x}_j$, $j = p, s$ defined in the same way as in section two (ω replaced by ωV_j),

$$
\tilde{x}_j(x) = x - \frac{i}{\omega V_j}\int_0^x d(s)\,ds, \quad j = p, s.
$$

Moreover, it can be shown that $\tilde{U}_j$, $j = p, s$, satisfies

1) $\tilde{U}_j \equiv U_j$, for $j = p, s$ in the left half-space $x \le 0$ (no reflection).
2) $\tilde{U}_j$, $j = p, s$, is damped in the right half-space.
3) the damping coefficient in the absorbing layer is

$$
\begin{aligned}
\frac{\|\tilde{U}_p(x)\|}{\|U_p(x)\|} &= \exp\left[-\frac{\cos\theta}{V_p}\int_0^x d(s)\,ds\right],\\
\frac{\|\tilde{U}_s(x)\|}{\|U_s(x)\|} &= \exp\left[-\frac{\cos\theta}{V_s}\int_0^x d(s)\,ds\right].
\end{aligned}
$$

Finite absorbing layer.—In practice, we take a finite absorbing layer by introducing a boundary at $x = \delta$, with a Dirichlet condition. This new boundary produces a reflection, but because the wave decreases exponentially in the layer, the reflection coefficient quickly becomes very small. This coefficient depends on the choice of $d(x)$ and on the size δ of the layer. To study the properties of the model in this case, we recall some classical results for the elastodynamic problem.

Consider the elastodynamic problem with a homogeneous Dirichlet condition($\mathbf{v} = 0$) on the boundary $x = 0$, as shown in Figure 1. Take, for example, the case of an incident plane wave P:

$$
U_p^{inc} = A_{inc}\mathbf{d}_p \exp\left[i\omega V_p\left(t - \frac{\mathbf{d}_p \cdot \mathbf{x}}{V_p}\right)\right], \mathbf{d}_p = (\cos\theta, \sin\theta).
$$

We know then (compare Achenbach [1984], Vol. 1, §5.6, p. 173) that the incident wave is reflected into a pressure wave U_p^r and a shear wave U_s^r, given by

$$
\begin{aligned}
U_p^r &= A_p^r \mathbf{d}_p^r \exp\left[i\omega V_p\left(t - \frac{\mathbf{d}_p^r \cdot \mathbf{x}}{V_p}\right)\right],\\
\mathbf{d}_p^r &= (-\cos\theta_1, \sin\theta_1),\\
U_s^r &= A_s^r \mathbf{d}_s^r \exp\left[i\omega V_p\left(t - \frac{\mathbf{p}_s \cdot \mathbf{x}}{V_p}\right)\right],\\
\mathbf{d}_s^r &= (-\sin\theta_2, \cos\theta_2),\\
\mathbf{p}_s &= (\cos\theta_2, \sin\theta_2),
\end{aligned}
$$

and we have the reflection coefficients

$$
\begin{aligned}
R_{pp} &= \frac{\|U_p^r\|}{\|U_p^{inc}\|} = \frac{\cos(\theta - \theta_2)}{\cos(\theta + \theta_2)},\\
R_{ps} &= \frac{\|U_s^r\|}{\|U_p^{inc}\|} = \frac{\sin\theta_2}{\cos(\theta + \theta_2)},
\end{aligned}
$$

with $\sin\theta_2 = V_s \sin\theta / V_p$. In the same way, in the case of an incident plane wave S, we have

$$
\begin{aligned}
R_{ss} &= \frac{\|U_s^r\|}{\|U_s^{inc}\|} = \frac{\sin(\theta + \theta_2)}{\sin(\theta - \theta_2)},\\
R_{sp} &= \frac{\|U_p^r\|}{\|U_s^{inc}\|} = \frac{\sin\theta_2}{\sin(\theta - \theta_2)},
\end{aligned}
$$

with $\cos\theta_2 = V_p \cos\theta / V_s$. We can consider now the case of the finite layer. Given that the plane waves U_j, $j = p, s$, corresponding to solutions of system (11), are given by equations (13), we can compute the reflection coefficients induced by the layer of width δ.

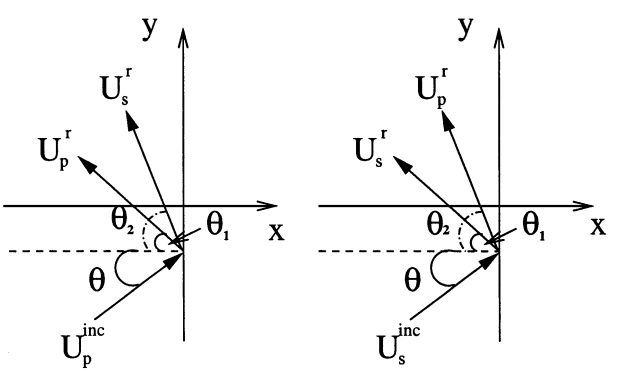

FIG. 1. Schematic view of the reflection of an incident P-wave (left) and of an incident S-wave (right) in the case of a homogeneous Dirichlet boundary condition.

The case of a plane wave *P*

As we have shown previously, there is no reflection at the interface $x=0$ when the plane wave $\tilde{U}_p$ penetrates the lossy medium. After traveling a length δ, we can compute $\tilde{U}_p$ by using formula (14), obtaining

$$\tilde{U}_p = U_p \exp\left[-\frac{\cos\theta}{V_p}\int_0^\delta d(s)\,ds\right].$$

Then plane wave $\tilde{U}_p$ gives at the boundary $x=\delta$, two reflected waves $\tilde{U}_p^r$ and $\tilde{U}_s^r$, which are damped until penetrating again the elastic medium at the interface $x=0$. It is easy to see that the reflection coefficient is given in this case by

$$R_{pp}^\delta = \frac{\|\tilde{U}_p^r(x)\|}{\|U_p(x)\|} = R_{pp}\exp\left[-2\frac{\cos\theta}{V_p}\int_0^\delta d(s)\,ds\right], x<0,$$
$$R_{ps}^\delta = \frac{\|\tilde{U}_s^r(x)\|}{\|U_p(x)\|} = R_{ps}\exp\left[-2\frac{\cos\theta}{V_p}\int_0^\delta d(s)\,ds\right], x<0. \tag{15}$$

The case of a plane wave *S*

In the case of an incident plane wave S, we obtain similarly

$$R_{ss}^\delta = \frac{\|\tilde{U}_s^r(x)\|}{\|U_s(x)\|} = R_{ss}\exp\left[-2\frac{\cos\theta}{V_s}\int_0^\delta d(s)\,ds\right], x<0,$$
$$R_{sp}^\delta = \frac{\|\tilde{U}_p^r(x)\|}{\|U_s(x)\|} = R_{sp}\exp\left[-2\frac{\cos\theta}{V_s}\int_0^\delta d(s)\,ds\right], x<0. \tag{16}$$

Relations (15) and (16) imply that the reflection can be made as weak as desired by choosing the damping factor $d(x)$ large enough. However, this is no longer true when we consider the discrete PML model. As we will see in Appendix A, the discrete absorbing layer model is not matched perfectly. That is a consequence of the numerical dispersion, which introduces a reflection at the interface.

The discrete PML model

In this section, we present the discrete PML model for elastodynamics. To do so, we introduce two numerical schemes for the discretization of system (11). The first is a finite-difference scheme, introduced in Virieux (1986), and the second is obtained using a new mixed finite element (Bécache et al., 1997) in a regular mesh. The use of this finite element has the advantage of leading to an explicit scheme (mass lumping), even in the case of an anisotropic elastic medium.

The Virieux finite-difference scheme

This scheme uses a staggered grid formulation, so that if v_x is computed at the points $(i,\,j)$ $(x_i = ih,\, y_j = jh)$ of a reference grid, then v_y is computed at the points $(i+\frac{1}{2},\, j+\frac{1}{2})$, σ_{xx} and σ_{yy} at $(i+\frac{1}{2},\, j)$, and σ_{xy} at $(i,\, j+\frac{1}{2})$. The discrete PML model associated to the Virieux finite-difference scheme can be written as follows:

$$(v_x)_{i,j}^n = (v_x^x)_{i,j}^n + (v_x^y)_{i,j}^n,$$

$$\frac{(v_x^x)_{i,j}^{n+1} - (v_x^x)_{i,j}^n}{\Delta t} + d_i^x\frac{(v_x^x)_{i,j}^{n+1} + (v_x^x)_{i,j}^n}{2} = \frac{(\sigma_{xx})_{i+\frac{1}{2},j}^{n+\frac{1}{2}} - (\sigma_{xx})_{i-\frac{1}{2},j}^{n+\frac{1}{2}}}{\varrho h},$$

$$\frac{(v_x^y)_{i,j}^{n+1} - (v_x^y)_{i,j}^n}{\Delta t} + d_j^y\frac{(v_x^y)_{i,j}^{n+1} + (v_x^y)_{i,j}^n}{2} = \frac{(\sigma_{xy})_{i,j+\frac{1}{2}}^{n+\frac{1}{2}} - (\sigma_{xy})_{i,j-\frac{1}{2}}^{n+\frac{1}{2}}}{\varrho h},$$

$$(v_y)_{i+\frac{1}{2},j+\frac{1}{2}}^n = (v_y^x)_{i+\frac{1}{2},j+\frac{1}{2}}^n + (v_y^y)_{i+\frac{1}{2},j+\frac{1}{2}}^n,$$

$$\frac{(v_y^x)_{i+\frac{1}{2},j+\frac{1}{2}}^{n+1} - (v_y^x)_{i+\frac{1}{2},j+\frac{1}{2}}^n}{\Delta t} + d_{i+\frac{1}{2}}^x\frac{(v_y^x)_{i+\frac{1}{2},j+\frac{1}{2}}^{n+1} + (v_y^x)_{i+\frac{1}{2},j+\frac{1}{2}}^n}{2} = \frac{(\sigma_{xy})_{i+1,j+\frac{1}{2}}^{n+\frac{1}{2}} - (\sigma_{xy})_{i,j+\frac{1}{2}}^{n+\frac{1}{2}}}{\varrho h},$$

$$\frac{(v_y^y)_{i+\frac{1}{2},j+\frac{1}{2}}^{n+1} - (v_y^y)_{i+\frac{1}{2},j+\frac{1}{2}}^n}{\Delta t} + d_{j+\frac{1}{2}}^y\frac{(v_y^y)_{i+\frac{1}{2},j+\frac{1}{2}}^{n+1} + (v_y^y)_{i+\frac{1}{2},j+\frac{1}{2}}^n}{2} = \frac{(\sigma_{yy})_{i+\frac{1}{2},j+1}^{n+\frac{1}{2}} - (\sigma_{xy})_{i+\frac{1}{2},j}^{n+\frac{1}{2}}}{\varrho h},$$

$$(\sigma_{xx})_{i+\frac{1}{2},j}^{n+\frac{1}{2}} = (\sigma_{xx}^x)_{i+\frac{1}{2},j}^{n+\frac{1}{2}} + (\sigma_{xx}^y)_{i+\frac{1}{2},j}^{n+\frac{1}{2}},$$

$$\frac{(\sigma_{xx}^x)_{i+\frac{1}{2},j}^{n+\frac{1}{2}} - (\sigma_{xx}^x)_{i+\frac{1}{2},j}^{n-\frac{1}{2}}}{\Delta t} + d_{i+\frac{1}{2}}^x\frac{(\sigma_{xx}^x)_{i+\frac{1}{2},j}^{n+\frac{1}{2}} + (\sigma_{xx}^x)_{i+\frac{1}{2},j}^{n-\frac{1}{2}}}{2} = (\lambda+2\mu)\frac{(v_x)_{i+1,j}^n - (v_x)_{i,j}^n}{h},$$

$$\frac{(\sigma_{xx}^y)_{i+\frac{1}{2},j}^{n+\frac{1}{2}} - (\sigma_{xx}^y)_{i+\frac{1}{2},j}^{n-\frac{1}{2}}}{\Delta t} + d_j^y\frac{(\sigma_{xx}^y)_{i+\frac{1}{2},j}^{n+\frac{1}{2}} + (\sigma_{xx}^y)_{i+\frac{1}{2},j}^{n-\frac{1}{2}}}{2} = \lambda\frac{(v_y)_{i+\frac{1}{2},j+\frac{1}{2}}^n - (v_y)_{i+\frac{1}{2},j-\frac{1}{2}}^n}{h},$$

$$(\sigma_{yy})_{i+\frac{1}{2},j}^{n+\frac{1}{2}} = (\sigma_{yy}^x)_{i+\frac{1}{2},j}^{n+\frac{1}{2}} + (\sigma_{yy}^y)_{i+\frac{1}{2},j}^{n+\frac{1}{2}},$$

$$\frac{(\sigma_{yy}^x)_{i+\frac{1}{2},j}^{n+\frac{1}{2}} - (\sigma_{yy}^x)_{i+\frac{1}{2},j}^{n-\frac{1}{2}}}{\Delta t} + d_{i+\frac{1}{2}}^x\frac{(\sigma_{yy}^x)_{i+\frac{1}{2},j}^{n+\frac{1}{2}} + (\sigma_{yy}^x)_{i+\frac{1}{2},j}^{n-\frac{1}{2}}}{2}$$

$$= \lambda \frac{(v_x)^n_{i1,j} - (v_x)^n_{i,j}}{h},$$

$$\frac{\left(\sigma^y_{yy}\right)^{n+\frac{1}{2}}_{i\frac{1}{2},j} - \left(\sigma^y_{yy}\right)^{n-\frac{1}{2}}_{i\frac{1}{2},j}}{\Delta t} + d^y_j \frac{\left(\sigma^y_{yy}\right)^{n+\frac{1}{2}}_{i\frac{1}{2},j} + \left(\sigma^y_{yy}\right)^{n-\frac{1}{2}}_{i\frac{1}{2},j}}{2}$$

$$= (\lambda + 2\mu) \frac{(v_y)^n_{i\frac{1}{2},j\frac{1}{2}} - (v_y)^n_{i\frac{1}{2},j-\frac{1}{2}}}{h},$$

$$\left(\sigma_{xy}\right)^{n+\frac{1}{2}}_{i,j\frac{1}{2}} = \left(\sigma^x_{xy}\right)^{n+\frac{1}{2}}_{i,j\frac{1}{2}} + \left(\sigma^y_{xy}\right)^{n+\frac{1}{2}}_{i,j\frac{1}{2}},$$

$$\frac{\left(\sigma^x_{xy}\right)^{n+\frac{1}{2}}_{i,j\frac{1}{2}} - \left(\sigma^x_{xy}\right)^{n-\frac{1}{2}}_{i,j\frac{1}{2}}}{\Delta t} + d^x_i \frac{\left(\sigma^x_{xy}\right)^{n+\frac{1}{2}}_{i,j\frac{1}{2}} + \left(\sigma^x_{xy}\right)^{n-\frac{1}{2}}_{i,j\frac{1}{2}}}{2}$$

$$= \mu \frac{(v_y)^n_{i\frac{1}{2},j\frac{1}{2}} - (v_y)^n_{i-\frac{1}{2},j\frac{1}{2}}}{h},$$

$$\frac{\left(\sigma^y_{xy}\right)^{n+\frac{1}{2}}_{i,j\frac{1}{2}} - \left(\sigma^y_{xy}\right)^{n-\frac{1}{2}}_{i,j\frac{1}{2}}}{\Delta t} + d^y_{j\frac{1}{2}} \frac{\left(\sigma^y_{xy}\right)^{n+\frac{1}{2}}_{i,j\frac{1}{2}} + \left(\sigma^y_{xy}\right)^{n-\frac{1}{2}}_{i,j\frac{1}{2}}}{2}$$

$$= \mu \frac{(v_x)^n_{i,j1} - (v_x)^n_{i,j}}{h},$$

where we used the notation $i^k = i + k$ and $j^k = j + k$.

The previous system of equations corresponds to the PML model in the corners, where we need damping in both directions. For the computation of the solution inside the PML layers in the x direction, we use the same system of equations with $d^y = 0$, and for PML layers in the y direction, we take $d^x = 0$. We present, in Figure 2, the values of d^x and d^y for the different PML layers.

THE FINITE-ELEMENT SCHEME

For this scheme, the velocity is approximated by piecewise constant functions and the stress tensor σ by piecewise linear functions with some particular continuity properties. More precisely, σ_{xy} is continuous in both directions and σ_{xx} (resp. σ_{yy}) is continuous only in the x (resp. y) direction. We present, in Figure 3, the mixed finite element used. On a regular grid, the velocity $v = (v_x, v_y)$ is computed at the points $(i^{\frac{1}{2}}, j^{\frac{1}{2}})$ and the stress tensor at the points (i, j). We consider the general case of an anisotropic elastic material described by the elasticity matrix C, and we denote by A the inverse of C

$$A = C^{-1} = \begin{bmatrix} a_{11} & a_{12} & a_{13} \\ a_{12} & a_{22} & a_{23} \\ a_{13} & a_{23} & a_{33} \end{bmatrix}.$$

The numerical scheme then can be written in the following way [see Bécache et al. (1998) for details]. For the first equation of system (11), we have

$$\frac{(v_x)^{n+1}_{i\frac{1}{2},j\frac{1}{2}} - (v_x)^n_{i\frac{1}{2},j\frac{1}{2}}}{\Delta t} = \frac{1}{2\varrho h}\Bigg(\left(\sigma^h_{xx}\right)^{n+\frac{1}{2}}_{i1,j} - \left(\sigma^h_{xx}\right)^{n+\frac{1}{2}}_{i,j} + \left(\sigma^b_{xx}\right)^{n+\frac{1}{2}}_{i1,j1} - \left(\sigma^b_{xx}\right)^{n+\frac{1}{2}}_{i,j1} + \left(\sigma_{xy}\right)^{n+\frac{1}{2}}_{i,j1} - \left(\sigma_{xy}\right)^{n+\frac{1}{2}}_{i,j} + \left(\sigma_{xy}\right)^{n+\frac{1}{2}}_{i1,j1} - \left(\sigma_{xy}\right)^{n+\frac{1}{2}}_{i1,j} \Bigg),$$

$$\frac{(v_y)^{n+1}_{i\frac{1}{2},j\frac{1}{2}} - (v_y)^n_{i\frac{1}{2},j\frac{1}{2}}}{\Delta t} = \frac{1}{2\varrho h}\Bigg(\left(\sigma_{xy}\right)^{n+\frac{1}{2}}_{i1,j} - \left(\sigma_{xy}\right)^{n+\frac{1}{2}}_{i,j} + \left(\sigma_{xy}\right)^{n+\frac{1}{2}}_{i1,j1} - \left(\sigma_{xy}\right)^{n+\frac{1}{2}}_{i,j1} + \left(\sigma^d_{yy}\right)^{n+\frac{1}{2}}_{i,j1} - \left(\sigma^d_{yy}\right)^{n+\frac{1}{2}}_{i,j} + \left(\sigma^g_{yy}\right)^{n+\frac{1}{2}}_{i1,j1} - \left(\sigma^g_{yy}\right)^{n+\frac{1}{2}}_{i1,j} \Bigg).$$

The second equation of system (11) results in the following 5×5 local system, coupling the five degrees of freedom associated to σ at each vertex (see Figure 3).

$$\frac{\Sigma^{n+\frac{1}{2}}_{i,j} - \Sigma^{n-\frac{1}{2}}_{i,j}}{\Delta t} = A_h^{-1} B_h^x + A_h^{-1} B_h^y,$$

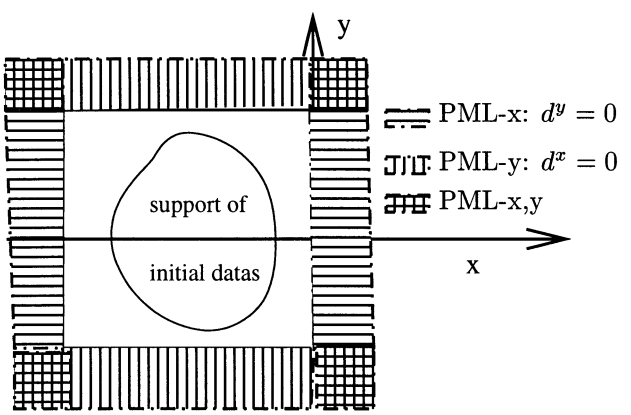

FIG. 2. The different PML layers: In the corners, both d^x and d^y are positive, and $d^y = 0$ (resp. $d^x = 0$) inside the PML layers in the x (resp. y) direction.

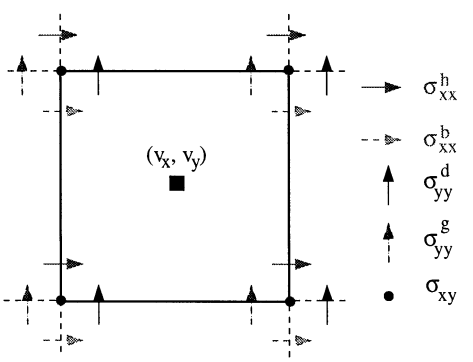

FIG. 3. The finite element: for the stress tensor, five degrees of freedom are associated at each summit of the element, and for the velocity, two degrees of freedom are associated at the center of the element.

where

$$\Sigma = \left[\sigma_{xx}^h, \sigma_{xx}^b, \sigma_{yy}^d, \sigma_{yy}^g, \sigma_{xy}\right]^t,$$

$$A_h = \frac{1}{2}\begin{bmatrix} 2a_{11} & 0 & a_{12} & a_{12} & 2a_{13} \\ 0 & 2a_{11} & a_{12} & a_{12} & 2a_{13} \\ a_{12} & a_{12} & 2a_{22} & 0 & 2a_{23} \\ a_{12} & a_{12} & 0 & 2a_{22} & 2a_{23} \\ 2a_{13} & 2a_{13} & 2a_{23} & 2a_{23} & 4a_{33} \end{bmatrix},$$

and

$$B_h^x = \frac{1}{h}\left[B_1^x, B_2^x, 0, 0, B_5^x\right]^t,$$

$$B_h^y = \frac{1}{h}\left[0, 0, B_3^y, B_4^y, B_5^y\right]^t,$$

with

$$\begin{aligned}
B_1^x &= (v_x)^n_{i\frac{1}{2},j\frac{1}{2}} - (v_x)^n_{i-\frac{1}{2},j\frac{1}{2}}, \\
B_2^x &= (v_x)^n_{i\frac{1}{2},j-\frac{1}{2}} - (v_x)^n_{i-\frac{1}{2},j-\frac{1}{2}}, \\
B_3^y &= (v_y)^n_{i\frac{1}{2},j\frac{1}{2}} - (v_y)^n_{i\frac{1}{2},j-\frac{1}{2}}, \\
B_4^y &= (v_y)^n_{i-\frac{1}{2},j\frac{1}{2}} - (v_y)^n_{i-\frac{1}{2},j-\frac{1}{2}}, \\
B_5^x &= (v_y)^n_{i\frac{1}{2},j\frac{1}{2}} - (v_y)^n_{i-\frac{1}{2},j\frac{1}{2}} + (v_y)^n_{i\frac{1}{2},j-\frac{1}{2}} - (v_y)^n_{i-\frac{1}{2},j-\frac{1}{2}}, \\
B_5^y &= (v_x)^n_{i\frac{1}{2},j\frac{1}{2}} - (v_x)^n_{i\frac{1}{2},j-\frac{1}{2}} + (v_x)^n_{i-\frac{1}{2},j\frac{1}{2}} - (v_x)^n_{i-\frac{1}{2},j-\frac{1}{2}}.
\end{aligned}$$

In the case of an isotropic elastic material, the matrix A_h^{-1} is given by

$$A_h^{-1} = \begin{bmatrix} a & c & b & b & 0 \\ c & a & b & b & 0 \\ b & b & a & c & 0 \\ b & b & c & a & 0 \\ 0 & 0 & 0 & 0 & d \end{bmatrix},$$

with

$$\begin{aligned}
a &= \frac{2(\lambda+2\mu)^2 - \lambda^2}{2(\lambda+2\mu)}, \quad b = \frac{\lambda}{2}, \\
c &= \frac{\lambda^2}{2(\lambda+2\mu)}, \quad d = \frac{\mu}{2}.
\end{aligned} \tag{17}$$

We now can write the PML model associated to this scheme, using the same technique as for the Virieux scheme,

$$(v_x)^n_{i\frac{1}{2},j\frac{1}{2}} = \left(v_x^x\right)^n_{i\frac{1}{2},j\frac{1}{2}} + \left(v_x^y\right)^n_{i\frac{1}{2},j\frac{1}{2}},$$

$$\frac{\left(v_x^x\right)^{n+1}_{i\frac{1}{2},j\frac{1}{2}} - \left(v_x^x\right)^n_{i\frac{1}{2},j\frac{1}{2}}}{\Delta t} + d^x_{i\frac{1}{2}} \frac{\left(v_x^x\right)^{n+1}_{i\frac{1}{2},j\frac{1}{2}} + \left(v_x^x\right)^n_{i\frac{1}{2},j\frac{1}{2}}}{2}$$

$$= \frac{1}{2\varrho h}\left(\left(\sigma_{xx}^h\right)^{n+\frac{1}{2}}_{i1,j} - \left(\sigma_{xx}^h\right)^{n+\frac{1}{2}}_{i,j} + \left(\sigma_{xx}^b\right)^{n+\frac{1}{2}}_{i1,j1} - \left(\sigma_{xx}^b\right)^{n+\frac{1}{2}}_{i,j1}\right),$$

$$\frac{\left(v_x^y\right)^{n+1}_{i\frac{1}{2},j\frac{1}{2}} - \left(v_x^y\right)^n_{i\frac{1}{2},j\frac{1}{2}}}{\Delta t} + d^y_{i\frac{1}{2}} \frac{\left(v_x^y\right)^{n+1}_{i\frac{1}{2},j\frac{1}{2}} + \left(v_x^y\right)^n_{i\frac{1}{2},j\frac{1}{2}}}{2}$$

$$= \frac{1}{2\varrho h}\left(\left(\sigma_{xy}\right)^{n+\frac{1}{2}}_{i,j1} - \left(\sigma_{xy}\right)^{n+\frac{1}{2}}_{i,j} + \left(\sigma_{xy}\right)^{n+\frac{1}{2}}_{i1,j1} - \left(\sigma_{xy}\right)^{n+\frac{1}{2}}_{i1,j}\right),$$

$$(v_y)^n_{i\frac{1}{2},j\frac{1}{2}} = \left(v_y^x\right)^n_{i\frac{1}{2},j\frac{1}{2}} + \left(v_y^y\right)^n_{i\frac{1}{2},j\frac{1}{2}},$$

$$\frac{\left(v_y^x\right)^{n+1}_{i\frac{1}{2},j\frac{1}{2}} - \left(v_y^x\right)^n_{i\frac{1}{2},j\frac{1}{2}}}{\Delta t} + d^x_{i\frac{1}{2}} \frac{\left(v_y^x\right)^{n+1}_{i\frac{1}{2},j\frac{1}{2}} + \left(v_y^x\right)^n_{i\frac{1}{2},j\frac{1}{2}}}{2}$$

$$= \frac{1}{2\varrho h}\left(\left(\sigma_{xy}\right)^{n+\frac{1}{2}}_{i1,j} - \left(\sigma_{xy}\right)^{n+\frac{1}{2}}_{i,j} + \left(\sigma_{xy}\right)^{n+\frac{1}{2}}_{i1,j1} - \left(\sigma_{xy}\right)^{n+\frac{1}{2}}_{i,j1}\right),$$

$$\frac{\left(v_y^y\right)^{n+1}_{i\frac{1}{2},j\frac{1}{2}} - \left(v_y^y\right)^n_{i\frac{1}{2},j\frac{1}{2}}}{\Delta t} + d^y_{i\frac{1}{2}} \frac{\left(v_y^y\right)^{n+1}_{i\frac{1}{2},j\frac{1}{2}} + \left(v_y^y\right)^n_{i\frac{1}{2},j\frac{1}{2}}}{2}$$

$$= \frac{1}{2\varrho h}\left(\left(\sigma_{yy}^d\right)^{n+\frac{1}{2}}_{i,j1} - \left(\sigma_{yy}^d\right)^{n+\frac{1}{2}}_{i,j} + \left(\sigma_{yy}^g\right)^{n+\frac{1}{2}}_{i1,j1} - \left(\sigma_{yy}^g\right)^{n+\frac{1}{2}}_{i1,j}\right),$$

and

$$\Sigma^{n+\frac{1}{2}}_{i,j} = \left(\Sigma^x\right)^{n+\frac{1}{2}}_{i,j} + \left(\Sigma^y\right)^{n+\frac{1}{2}}_{i,j},$$

$$\frac{\left(\Sigma^x\right)^{n+\frac{1}{2}}_{i,j} - \left(\Sigma^x\right)^{n-\frac{1}{2}}_{i,j}}{\Delta t} + d_i^x \frac{\left(\Sigma^x\right)^{n+\frac{1}{2}}_{i,j} + \left(\Sigma^x\right)^{n-\frac{1}{2}}_{i,j}}{2} = A_h^{-1} B_h^x,$$

$$\frac{\left(\Sigma^y\right)^{n+\frac{1}{2}}_{i,j} - \left(\Sigma^y\right)^{n-\frac{1}{2}}_{i,j}}{\Delta t} + d_i^y \frac{\left(\Sigma^y\right)^{n+\frac{1}{2}}_{i,j} + \left(\Sigma^y\right)^{n-\frac{1}{2}}_{i,j}}{2} = A_h^{-1} B_h^y.$$

The properties of this model are studied in terms of a numerical dispersion analysis presented in Appendix A. This analysis permits us to compute the reflection coefficients in the case of a homogeneous, isotropic elastic solid. In this case, we have found that the reflection coefficients are approximately proportional to h^2. That shows the second-order accuracy of the discrete PML model, which thus is no longer perfectly matched. This means in particular that the damping factor cannot be chosen to be too large with respect to the inverse of the discretization step. Of course, it must be large enough to allow the damping of the wave inside the layer, so there is a trade-off (see the end of the Appendix A for more details).

The theoretical results presented in the previous sections are based on a plane-wave analysis and thus can be applied only to wave-propagation problems in homogeneous media. However, as we will see in the next sections, the discrete PML model also can be used to compute numerically the solution of the elastodynamic problem in heterogeneous, anisotropic elastic media, although we have no theoretical justification for this extension.

NUMERICAL RESULTS

In the following examples, we simulate elastic wave propagation in a 2-D unbounded medium. We will present several results, including the case of heterogeneous, anisotropic elastic media. To show the generality of the method, we give some numerical results for both schemes: the Virieux finite-difference scheme and the finite-element scheme. A more complete analysis is presented for the finite-element scheme; namely, the

discrete reflection coefficients are computed as a function of the incident angle. Let us first set some notation and give the characteristics of the numerical examples that will follow. We consider an unbounded domain Ω in 2-D, occupied by an elastic material, and we suppose that the initial condition (or the source) is supported in a part of Ω. The material will be characterized by its wave velocities V_p (pressure) and V_s (shear) in the isotropic case and by its elasticity matrix C in the anisotropic case. To solve numerically the elastodynamic problem in Ω, we define a bounded domain D of a simple geometry (here it will be a square), containing the support of the initial data, with absorbing layers (PML) on all four boundaries. For the discretization of the problem, we take a regular grid on D composed of $N \times N$ square elements of edge $h = 1/N$. The time step then is computed following the CFL condition for each scheme. More precisely, we take: $\Delta t = 0.9h/(\sqrt{2}V_p)$ for the Virieux scheme and $\Delta t = h/V_p$ for the finite-element scheme.

For our numerical experiments, an explosive source located at point $S = (x^s, y^s)$ is used, that is,

$$f(x,t) = F(t)\mathbf{g}(r).$$

The function $F(t)$ is defined by

$$F(t) = \begin{cases} -2\pi^2 f_0^2 (t - t_0)\, e^{-\pi^2 f_0^2 (t-t_0)^2} & \text{if } t \le 2t_0 \\ 0 & \text{if } t > 2t_0 \end{cases}, \quad (18)$$

where $t_0 = 1/f_0$, $f_0 = Vs/(hN_L)$ is the central frequency, and N_L is the number of points per S wavelength. The function $\mathbf{g}(r)$ is a radial function given by

$$\mathbf{g}(r) = \left(1 - \frac{r^2}{a^2}\right)^3 1_{B_a}\left(\frac{x - x^s}{r}, \frac{y - y^s}{r}\right),$$
$$r = \sqrt{(x - x^s)^2 + (y - y^s)^2}, \quad a = 5h, \quad (19)$$

where 1_{B_a} is one on B_a, the disk of center S and radius a, and zero elsewhere. In the absorbing layers, we use the following model for the damping parameter $d(x)$,

$$d(x) = d_0 \left(\frac{x}{\delta}\right)^2, \quad (20)$$

where δ is the width of the layer and d_0 is a function of the theoretical reflection coefficient ($R = R_{pp}^{\delta}$) [see relation (15) for $\theta = 0$],

$$d_0 = \log\left(\frac{1}{R}\right)\frac{3V_p}{2\delta}. \quad (21)$$

We first present some results in a homogeneous isotropic medium.

Homogeneous, isotropic elastic medium, Virieux scheme

We consider here an elastic medium with $V_p = 2000$ m/s, $V_s = 1400$ m/s. The characteristics of the discretization are

$$N = 200, \quad h = 0.15 \text{ m}, \quad S = (7.5 \text{ m}, 7.5 \text{ m}),$$
$$N_L = 20, \quad \delta = 10\,h \quad \text{and} \quad R = 0.001.$$

We present some snapshots of the solution in Figure 4. The snapshots show no reflection when the results are presented on the normal scale. Indeed, for the PML model used in this example, the reflection coefficient is about 0.1%, as can be seen by magnifying the results by a factor of 100 (see Figure 5). In Figure 5, we also present the results obtained using the first-order absorbing boundary condition introduced by Reynolds (1978). The reflection coefficient for this ABC is about 10%; the first-order ABC is not accurate enough for waves traveling obliquely to the boundary.

Heterogeneous, isotropic elastic medium, Virieux scheme

We consider a heterogeneous elastic medium; the interface is parallel to the x axis and located in the middle of the frame (see Figure 6). The wave velocities in the two media are $V_p^1 = 2000$ m/s, $V_s^1 = 1400$ m/s (the upper medium), $V_p^2 = 1000$ m/s, $V_s^2 = 700$ m/s (the lower medium). All the other parameters are the same as in section A, where $V_s = (V_s^1 + V_s^2)/2$ has been used for the computation of f_0 (equation 18) and $V_p = V_p^1$ to compute Δt. The source now is located in the lower medium near the interface (at point [15m, 16.2m]). We present some snapshots of the solution in Figure 6. The reflection coefficient for this example is about 0.1%, as we can see in Figure 6.

Heterogeneous, isotropic elastic medium, finite-element scheme

The heterogeneous elastic medium considered here is characterized by the velocity model presented in Figure 7; we have

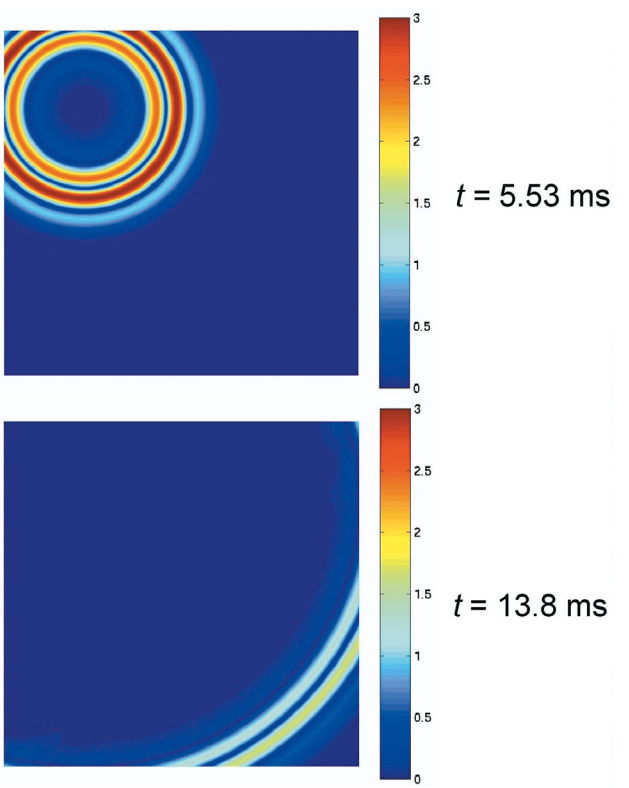

FIG. 4. Snapshots of 2-D elastic finite-difference simulations (Virieux scheme), in a homogeneous medium, using a PML layer with width $10h$. The snapshots are the norm of the velocity $\|v\| = \sqrt{v_1^2 + v_2^2}$.

max $V_p/\min V_p = 2.1$ and $V_p = 1.6V_s$. For the discretization, V_p and V_s are piecewise constants (one value per element). The size of the grid is 200×200, $h = 0.15$ m, $N_L = 10$, and the source is located at point (15 m, 3 m). We present, in Figure 8, the norm of the velocity magnified by a factor of 20 for three experiments corresponding to different absorbing layers. More precisely, relations (20) and (21) are used with $\delta = 5h - R = 0.01$, $\delta = 10h - R = 0.001$, and $\delta = 20h - R = 0.0001$. Let us recall that these values for R correspond to the theoretical (R_{pp}) reflection coefficients. The reflection coefficients obtained numerically are close to the theoretical ones. This is no longer true if the number of meshes inside the layer is too small; the smaller R, the larger layer width required. This phenomenon results from the numerical dispersion (Collino and Monk, 1998).

Homogeneous, anisotropic elastic medium, finite-element scheme

In this example, we consider an anisotropic elastic solid, the apatite. We want to point out that in the case of anisotropic elastic materials, only lower-order absorbing boundary conditions are known, and they are quite difficult to implement (Bécache, 1991). On the contrary, the generalization of the PML model to the anisotropic case is straightforward, and there are no supplementary difficulties for the implementation. Moreover, the results are very satisfactory, as we can see in the following figures.

The characteristics of the problem are $N = 200$, $h = 0.15$ m, and $N_L = 10$, and the source is located at the center of the frame $S = (15$ m, 15 m). We present in Figure 9 three experiments, corresponding to $\delta = 5h - R = 0.01$, $\delta = 10h - R = 0.001$, and $\delta = 20h - R = 0.0001$. We can see in Figure 9 that there is no reflection when the results are presented on the normal scale, as was already the case for a homogeneous medium. However, we can see some reflection by magnifying these results, as shown in Figure 10. The reflection coefficients obtained numerically are close to the theoretical ones.

Reflection coefficients

In this section, we show reflection coefficients computed by using numerical simulations. We consider a homogeneous isotropic elastic solid ($V_p = 5.710$ m/s, $V_s = 2.93$ m/s), and we use the finite-element scheme for the space discretization. To compute the reflection coefficients we first consider the solution of the elastodynamic problem at points M_i located near the

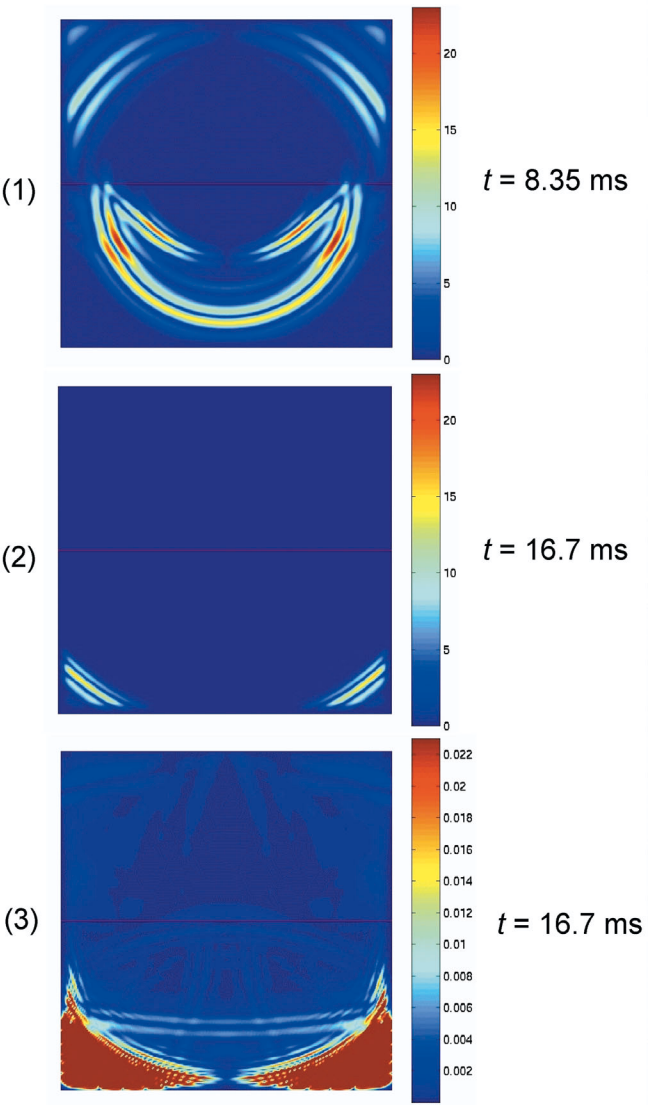

FIG. 6. Snapshots of 2-D elastic finite-differences simulations (Virieux scheme), in a heterogeneous medium, using a PML layer with length $10h$. We present the norm of the velocity $\|v\| = \sqrt{v_1^2 + v_2^2}$, in the normal scale (1) and (2). To see some reflections, (3) is magnified by a factor of 1000.

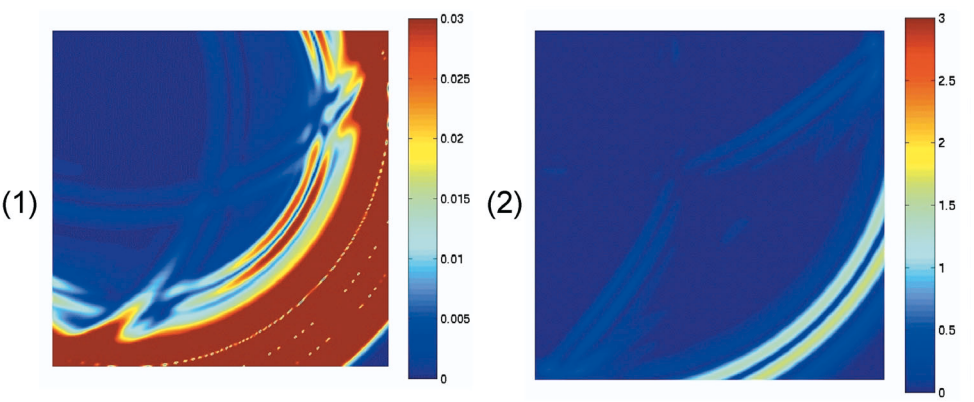

FIG. 5. The the norm of the velocity at $t = 13.8$ ms: In (1), we present the results obtained with the PML model ($\delta = 10h$) magnified by a factor of 100. In (2), we present the results obtained with a first-order ABC on the normal scale.

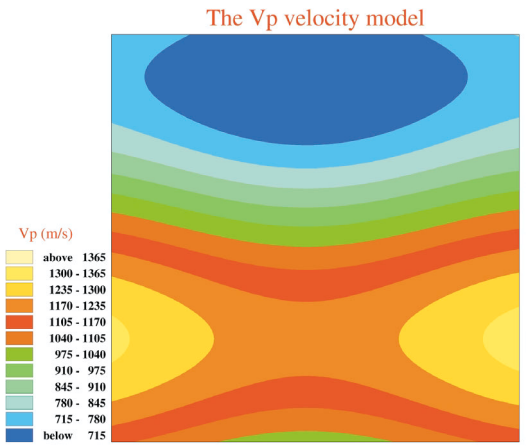

FIG. 7. The velocity model for the heterogeneous medium; $\max V_p/\min V_p = 2.1$ and $V_p = 1.6V_s$.

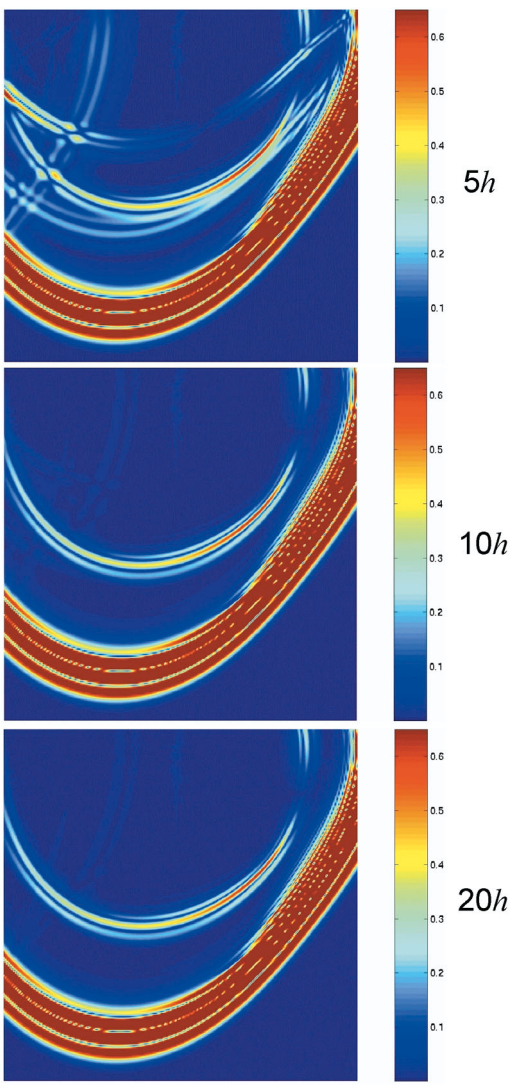

FIG. 8. Snapshots of 2-D elastic finite-elements simulations, in a heterogeneous, medium, using the PML absorbing layer model with $\delta = 5h$, $\delta = 10h$, and $\delta = 20h$. The snapshots are the norm of the velocity at $t = 14.2$ ms magnified by a factor of 20.

upper boundary of domain D_1 (D_1 is a rectangular domain of size 200 m $\times$ 100 m, and a PML layer model is used on all boundaries of the domain). We denote by $(V_1)_i$ the velocity vector at point M_i. Then to obtain a reference solution at points M_i, we move the upper boundary of the domain 50 m above. That is, we solve the elastodynamic problem in the domain D_2 (a rectangle of size 200 m $\times$ 150 m). We also use the PML layer model on all boundaries of the domain, and we denote by $(V_2)_i$ the velocity vector at point M_i. The geometry of the problem with the two computational domains is shown in Figure 11. In the case of a pure P-wave source, we define the reflection coefficients by

$$(R_{pp})(\theta_i) = \frac{\operatorname{div}(U_2)_i - \operatorname{div}(U_1)_i}{\operatorname{div}(U_2)_i},$$
$$(R_{ps})(\theta_i) = \frac{\operatorname{curl}(U_2)_i - \operatorname{curl}(U_1)_i}{\operatorname{curl}(U_2)_i}. \tag{22}$$

In the same way, we define

$$(R_{ss})(\theta_i) = \frac{\operatorname{curl}(U_2) - \operatorname{curl}(U_1)}{\operatorname{curl}(U_2)},$$
$$(R_{sp})(\theta_i) = \frac{\operatorname{div}(U_2) - \operatorname{div}(U_1)}{\operatorname{div}(U_2)},$$

in the case of a pure S-wave source. For our examples, we use the P-wave source function given by (18, 19) with $N_L = 16$. For this source function, the curl of the velocity is smaller than the

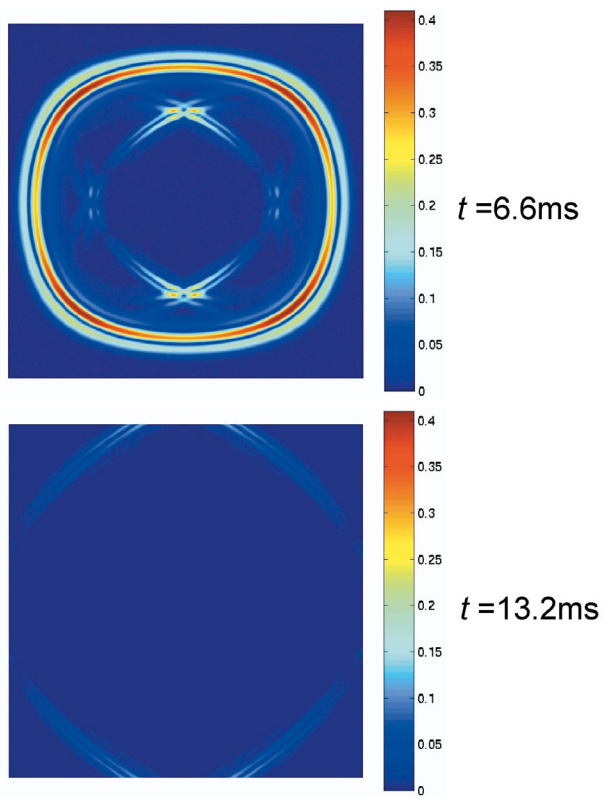

FIG. 9. Snapshots of 2-D elastic finite-elements simulations, in a homogeneous, anisotropic medium, using the PML absorbing layer model with $\delta = 5h$. The snapshots are the norm of the velocity $\|v\| = \sqrt{v_1^2 + v_2^2}$.

divergence by a factor 10^{-10}. The reflection coefficient R_{ps} is neglected.

Relation (22) is used to compute two reflection coefficients at each time step. The results presented in Figure 12 correspond to their mean value over $[0, T]$, for $T = 25$ s.

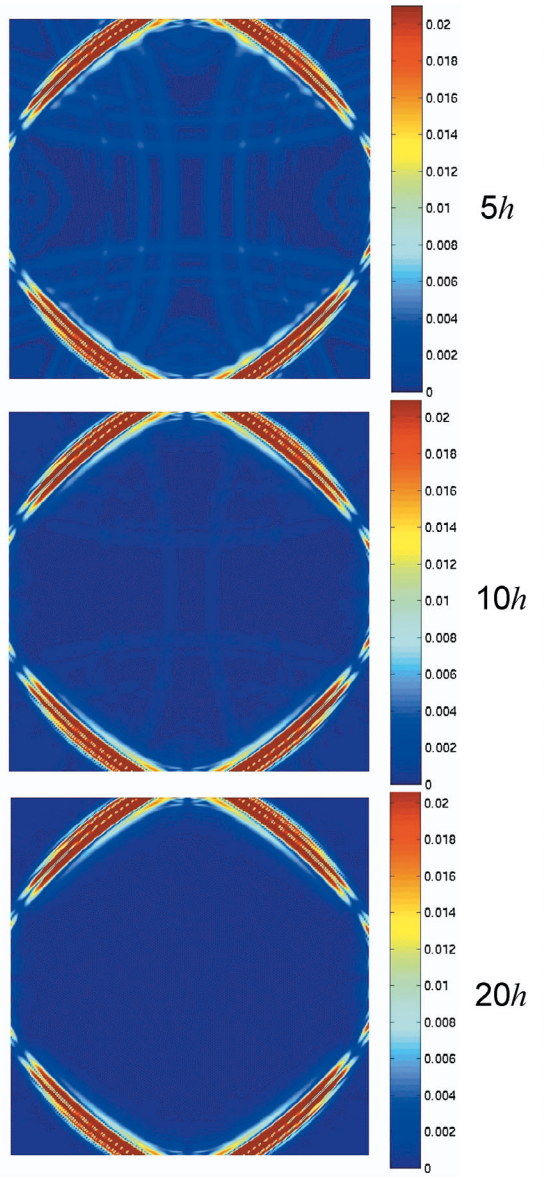

FIG. 10. Snapshots of 2-D elastic finite-elements simulations, in a homogeneous, anisotropic medium, using the PML absorbing layer model with $\delta = 5h, \delta = 10h$, and $\delta = 20h$. The snapshots are the norm of the velocity at $t = 13.2$ ms magnified by a factor of 20.

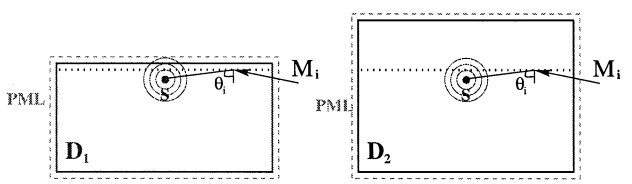

FIG. 11. Geometry for computing reflection coefficients. Two computational domains are defined: D_1 200 m × 100 m and D_2 200 m × 150 m.

The grid size is 400×200 for D_1, 400×300 for D_2, and $h = 0.5$ m for both domains. The source is located at point (200, 80) of the grid. In the PML layers,

$$d(x) = d_0 \left(\frac{x}{\delta}\right)^4, \tag{23}$$

where δ is the length of the layer and d_0 is given by

$$d_0 = \log\left(\frac{1}{R}\right)\frac{4V_p}{2\delta}.$$

We present three experiments with $\delta = 5h - R = 10^{-4}$, $\delta = 10h - R = 10^{-6}$, and $\delta = 20h - R = 10^{-8}$. To examine the performance of the PML model, comparisons with the first-, second-, and third-order Higdon's absorbing boundary conditions are performed.

The reflection coefficients for the absorbing boundary conditions proposed by Higdon are the theoretical ones. We obtain them by applying an operator of the form

$$\prod_{i=1}^{m}\left(\beta_i \frac{\partial}{\partial t} + V_p \frac{\partial}{\partial n}\right),$$

with $m = 1; \beta_1 = 1$, or $m = 2; \beta_1 = 1, \beta_2 = V_p/V_s (= 1.95)$, or $m = 3; \beta_1 = 1, \beta_2 = 1.5, \beta_3 = V_p/V_s (= 1.95)$.

As we can see in Figure 12, for almost all angles of incidence, the PML absorbing layer model gives better results then the absorbing boundary conditions of first and second order and this even for the $5h$ length absorbing layer. Compared with the third-order absorbing condition, the PML layers of $10h$ and $20h$ are substantially better except near the 60-degree angle. We want to point out that in this example we compare the reflection coefficients provided by the continuous Higdon model to the one given by the discrete PML model. It is known that the Higdon reflection coefficients increase when discretization is used.

The numerical results presented in the sections above show the generality of the PML model: These models can be implemented easily in different numerical schemes. They give satisfactory results even in the case of anisotropic, heterogeneous elastic media. The reflection coefficients are close to the theoretical ones for all the presented experiments. They are about 1% for a $5h$ PML layer width, 0.1% for a $10h$ PML layer width, and 0.01% for a $20h$ PML layer width in all experiments. In practice, one should choose the length of the layer

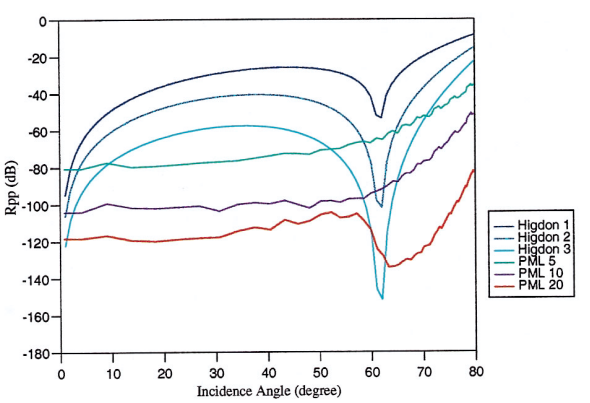

FIG. 12. Comparison of R_{pp} for the Higdon ABCs and PML.

as a function of the scale of the problem and the requested reflection coefficient. In the numerical examples we have presented, the scale of the problems was about 15 wavelengths of P-wave (λ_p) in each direction. In this case, a PML layer with $\delta = 5h$ (that is, about 0.5 λ_p) is sufficient and gives better results than the second-order absorbing condition. However, for larger-scale computations, the numerical dispersion will be more important, and thus a PML layer with $\delta = 5h$ probably would not give the expected results. Thus, for large-scale problems, one should consider a PML layer with $\delta \geq 10h$. We want to point out that even in this case, the additional cost remains modest, given that the layer represents only a small portion of the total grid. Let us finally remark that the PML model can be extended easily to the case of Rayleigh waves. (Experimental results not shown in this paper have demonstrated a good absorption of Rayleigh waves).

CONCLUSIONS

We have presented in this paper a generalization of the PML absorbing layer model for the elastodynamic problem in the case of heterogeneous, anisotropic media. The implementation of this model was presented in the 2-D case but it can be extended straightforwardly to the 3-D case. The superiority of this model compared with the absorbing boundary conditions proposed by Higdon was shown by numerical results in the case of an isotropic, homogeneous medium. Moreover, we have shown by several numerical examples the efficiency of this model even in the case of heterogeneous, anisotropic media. To conclude, let us point out the ease of the implementation of this model in the case of an anisotropic, elastic medium, in comparison with the complexity of the respective absorbing boundary conditions.

REFERENCES

Achenbach, J. D., 1984, Wave Propagation in Elastic Solids, Vols. I and II: Elsevier Science Publ. B.V.

Auld, B. A., 1973, Acoustic fields and elastic waves in solids: John Wiley & Sons, Inc.

Bécache, E., 1991, Résolution par une méthode d'équations intégrales d'un problème de diffraction d'ondes élastiques transitoires par une fissure.: Ph.D. Thesis, Univ. of Paris 6.

Bécache, E., Joly, P., and Tsogka, C., 1997, Eléments finis mixtes et condensation de masse en élastodynamique linéaire: (i) construction: C. R. Acad. Sci. Paris Sér. I Math., **325**, 545–550.

——— 1998, Fictitious domain method applied to the scattering by a crack of transient elastic waves in anisotropic media: A new family of mixed finite elements leading to explicit schemes: Mathematical and numerical aspects of wave propagation: SIAM, 322–326.

Bérenger, J., 1994, A perfectly matched layer for the absorption of electromagnetic waves: J. Comput. Phys., **114** 185–200.

——— 1996, Three-dimensional perfectly matched layer for the absorption of electromagnetic waves: J. Comput. Phys., **127**, 363–379.

——— 1997, Improved PML for the FDTD Solution of Wave-Structure Interaction Problems: IEEE Trans. Antennas and Propagation, **45**, 466–473.

Chalindar, B., 1987, Conditions aux limites artificielles pour les équations de l'élastodynamique: Ph.D. thesis, Univ. Saint-Étienne.

Collino, F., 1996, Perfectly matched absorbing layers for the paraxial equations: J. Comput. Phys., **131**, 164–180.

Collino, F., and Monk, P., 1998, Optimizing the perfectly matched layers: Comput. Methods Appl. Mech. Engrg., **164**, No. 1–2, 157–171.

Engquist, B., and Majda, A., 1997, Absorbing boundary conditions for the numerical simulation of Waves: Math. Comp., **31**, 629–651.

Hagstrom, T., 1997, On High-order radiation boundary condition, *in* Engquist, B., and Kriegsmann, G. A., Eds, Computational Wave Propagation: Springer-Verlag New York, Inc., **86**, 1–21.

Hastings, F., Schneider, J. B., and Broschat, S. L., 1996, Application of the perfectly matched layer (PML) absorbing boundary condition to elastic wave propagation: J. Acoust. Soc. Am., **100**, 3061–3069.

Higdon, R., 1990, Radiation boundary conditions for elastic wave propagation: SIAM J. Numer. Anal., **27**, 831–870.

——— 1991, Absorbing boundary conditions for elastic waves: Geophysics, **56**, 231–241.

——— 1992, Absorbing boundary conditions for acoustic and elastic waves in stratified media: J. Comput. Phys., **101**, 386–418.

Israeli, M., and Orszag, S., 1981, Approximation of radiation boundary conditions: J. Comput. Phys., **41**, 115–135.

Peng, C., and Toksoz, M., 1995, An optimal absorbing boundary condition for elastic wave modeling: Geophysics, **60**, 296–301.

Rappaport, C., 1995, Perfectly matched absorbing conditions based on anisotropic lossy mapping of space, IEEE Microwave and Guided Wave Letters, **5**, No. 3, 90–92.

Reynolds, A., 1978, Boundary conditions for the numerical solution of wave propagation problems: Geophysics, **43** 1099–1110.

Simone, A., and Hestholm, S., 1998, Instability in applying absorbing boundary conditions to high-order seismic modeling algorithms: Geophysics, **63**, 1017–1023.

Sochacki, J., Kubichek, R., George, J., Fletcher, W., and Smithson, S., 1987, Absorbing boundary conditions and surface waves: Geophysics: **52**, 60–71.

Teixeira, F. L., and Chew, W. C., 1998, Analytical derivation of a conformal perfectly matched absorber for electromagnetic waves: Micro. Opt. Tech. Lett., **17**, 231–236.

Turkel, E., and Yefet, A., 1998, Absorbing pml boundary layers for wave-like equations. Absorbing boundary conditions: Appl. Numer. Math., **27**, No. 4, 553–557.

Virieux, J., 1986, P-sv wave propagation in heterogeneous media: Velocity-stress finite difference method: Geophysics, **51**, 889–901.

Zhao, L., and Cangellaris, A. C., 1996, A general approach for developing unsplit-field time-domain implementations of perfectly matched layers for FDTD grid truncation: IEEE Trans. Microwave Theory Tech., **44**, 2555–2563.

APPENDIX A
DISPERSION ANALYSIS

In this section, we will study the properties of the discrete PML model for elastodynamics in terms of a numerical dispersion analysis, that is, a plane-wave analysis. We present this analysis only for the finite-element scheme. We consider the case of a homogeneous, isotropic elastic medium characterized by the Lamé coefficients λ, μ and the density ϱ. We use an infinite PML layer in the x-direction. We look for plane-wave solutions of the form

$$(V^\ell)^{n+\frac{1}{2}}_{i\frac{1}{2},j\frac{1}{2}} = (\hat{V}^\ell)_{i\frac{1}{2}} \exp\left[-ik_y\left(j\tfrac{1}{2}\right)h + i\omega\left(n+\frac{1}{2}\right)\Delta t\right],$$
$$(\Sigma^\ell)^n_{i,j} = (\hat{\Sigma}^\ell)_i \exp[-ik_y jh + i\omega n\Delta t],$$
$$V^\ell = \left[v_x^\ell, v_y^\ell\right]^T,\ \Sigma^\ell = \left[\sigma_{xx}^{h,\ell}, \sigma_{xx}^{b,\ell}, \sigma_{yy}^{d,\ell}, \sigma_{yy}^{g,\ell}, \sigma_{xy}^{\ell}\right]^T,$$

for $\ell = \perp, \parallel$, and we set

$$(\hat{V})_{i\frac{1}{2}} = (\hat{V}^\parallel)_{i\frac{1}{2}} + (\hat{V}^\perp)_{i\frac{1}{2}};\ (\hat{\Sigma})_i = (\hat{\Sigma}^\parallel)_i + (\hat{\Sigma}^\perp)_i$$

Plugging these expressions into the discrete scheme and eliminating the unknowns associated to σ lead to

$$\frac{A_t^2}{\Delta t^2}(\hat{v}_x)_{i\frac{1}{2}} = \frac{\mu}{\varrho}A_y^2\frac{(\hat{v}_x)_{i\frac{3}{2}} + 2(\hat{v}_x)_{i\frac{1}{2}} + (\hat{v}_x)_{i-\frac{1}{2}}}{4h^2}$$
$$+\frac{a + c\cos(k_y h)}{\varrho D_{i\frac{1}{2}}}\left(\frac{(\hat{v}_x)_{i\frac{3}{2}} - (\hat{v}_x)_{i\frac{1}{2}}}{h^2 D_{i1}} - \frac{(\hat{v}_x)_{i\frac{1}{2}} - (\hat{v}_x)_{i-\frac{1}{2}}}{h^2 D_i}\right) - A_y\frac{\mu}{\varrho}\cos\left(\frac{k_y h}{2}\right)$$
$$\times\left(\frac{(\hat{v}_y)_{i\frac{3}{2}} - (\hat{v}_y)_{i\frac{1}{2}}}{2h^2 D_{i1}} + \frac{(\hat{v}_y)_{i\frac{1}{2}} - (\hat{v}_y)_{i-\frac{1}{2}}}{2h^2 D_i} + \frac{(\hat{v}_y)_{i\frac{3}{2}} - (\hat{v}_y)_{i-\frac{1}{2}}}{h^2 D_{i\frac{1}{2}}}\right), \tag{A-1}$$

$$\frac{A_t^2}{\Delta t^2}(\hat{v}_y)_{i\frac{1}{2}} = \frac{1}{\varrho}A_y^2\frac{c(\hat{v}_y)_{i\frac{3}{2}} + 2a(\hat{v}_y)_{i\frac{1}{2}} + c(\hat{v}_y)_{i-\frac{1}{2}}}{2h^2}$$
$$+\frac{\mu}{\varrho}\cos^2\left(\frac{k_y h}{2}\right)\left(\frac{(\hat{v}_y)_{i\frac{3}{2}} - (\hat{v}_y)_{i\frac{1}{2}}}{h^2 D_{i1} D_{i\frac{1}{2}}} - \frac{(\hat{v}_y)_{i\frac{1}{2}} - (\hat{v}_y)_{i-\frac{1}{2}}}{h^2 D_i D_{i\frac{1}{2}}}\right) - A_y\frac{b}{\varrho}\cos\left(\frac{k_y h}{2}\right)$$
$$\times\left(\frac{(\hat{v}_x)_{i\frac{3}{2}} - (\hat{v}_x)_{i\frac{1}{2}}}{h^2 D_{i1}} + \frac{(\hat{v}_x)_{i\frac{1}{2}} - (\hat{v}_x)_{i-\frac{1}{2}}}{h^2 D_i} + \frac{(\hat{v}_x)_{i\frac{3}{2}} - (\hat{v}_x)_{i-\frac{1}{2}}}{2h^2 D_{i\frac{1}{2}}}\right), \tag{A-2}$$

where a, b, c are given by (17) and A_t, A_y, C_ℓ, and D_ℓ are defined by

$$A_t = 2i\sin\left(\frac{\omega\Delta t}{2}\right),\quad A_y = 2i\sin\left(\frac{k_y h}{2}\right),$$
$$C_\ell = 2i\sin\left(\frac{\omega\Delta t}{2}\right) + d_\ell\Delta t\cos\left(\frac{\omega\Delta t}{2}\right),\quad \ell = i, i\tfrac{1}{2},$$
$$D_\ell = \frac{C_\ell}{A_t},\ \ell = i, i\tfrac{1}{2}.$$

Let us consider now the case of a medium with a unique infinite layer for which

$$d_i = \begin{cases} 0 & \text{if } i \le 0 \\ d_\infty & \text{if } i > 0 \end{cases},\quad d_{i\frac{1}{2}} = \begin{cases} 0 & \text{if } i < 0 \\ d_\infty & \text{if } i > 0 \end{cases},$$

$d_{\frac{1}{2}}$ remaining undetermined yet, and let us look for particular solution of the form (see Figure A-1)

P-wave

$$(\hat{V})_{i\frac{1}{2}} = \mathbf{d}_p\, e^{-ik_x\left(i\frac{1}{2}\right)h} + R_{pp}\mathbf{d}_p^r e^{ik_x\left(i\frac{1}{2}\right)h} + R_{ps}\mathbf{d}_s^r e^{ik_x\left(i\frac{1}{2}\right)h} \quad \text{for } i\tfrac{1}{2} \le 0,$$
$$(\hat{V})_{i\frac{1}{2}} = T_{pp}\tilde{d}_p e^{-i\tilde{k}_x\left(i\frac{1}{2}\right)h} + T_{ps}\tilde{d}_s e^{-i\tilde{k}_x\left(i\frac{1}{2}\right)h} \text{ for } i\tfrac{1}{2} \ge 0.$$

S-wave

$$(\hat{V})_{i\frac{1}{2}} = \mathbf{d}_s e^{-ik_x\left(i\frac{1}{2}\right)h} + R_{ss}\mathbf{d}_s^r e^{ik_x\left(i\frac{1}{2}\right)h} + R_{sp}\mathbf{d}_p^r e^{ik_x\left(i\frac{1}{2}\right)h} \quad \text{for } i\tfrac{1}{2} \le 0,$$
$$(\hat{V})_{i\frac{1}{2}} = T_{ss}\tilde{\mathbf{d}}_s e^{-i\tilde{k}_x\left(i\frac{1}{2}\right)h} + T_{sp}\tilde{\mathbf{d}}_p e^{-i\tilde{k}_x\left(i\frac{1}{2}\right)h} \text{ for } i\tfrac{1}{2} \ge 0.$$

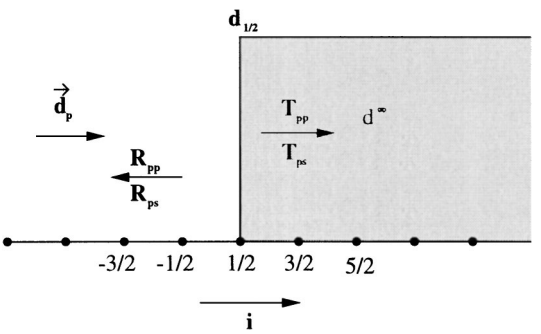

FIG. A-1. Schematic view of the plane-wave solution in a single-layer discrete model.

Equations (A-1) and (A-2) are satisfied for $i^{\frac{1}{2}} \neq 0$ if k_x and $\tilde{k}_x$ are solutions of the two relations of dispersion (A-3) (free medium) and (A-4) (lossy medium).

$$\frac{X_t^2}{\Delta t^2}\begin{bmatrix}\hat{v}_x\\ \hat{v}_y\end{bmatrix} = \frac{1}{h^2}\begin{bmatrix}\hat{K}_{11} & \hat{K}_{12}\\ \hat{K}_{12} & \hat{K}_{22}\end{bmatrix}\begin{bmatrix}\hat{v}_x\\ \hat{v}_y\end{bmatrix}, \tag{A-3}$$

$$\frac{X_t^2}{\Delta t^2}\begin{bmatrix}\hat{v}_x\\ \hat{v}_y\end{bmatrix} = \frac{1}{h^2}\begin{bmatrix}\tilde{K}_{11} & \tilde{K}_{12}\\ \tilde{K}_{12} & \tilde{K}_{22}\end{bmatrix}\begin{bmatrix}\hat{v}_x\\ \hat{v}_y\end{bmatrix}, \tag{A-4}$$

with

$$\begin{aligned}
\hat{K}_{11} &= V_p^2 X_x(1-4\alpha X_y) + V_s^2 X_y(1-\beta X_x),\\
\hat{K}_{22} &= V_p^2 X_y(1-4\alpha X_x) + V_s^2 X_x(1-\beta X_y),\\
\hat{K}_{12} &= \left(V_p^2 - V_s^2\right)\sqrt{X_x X_y(1-X_x)(1-X_y)},\\
X_t &= \sin^2\left(\frac{\omega\Delta t}{2}\right), \quad X_x = \sin^2\left(\frac{k_x h}{2}\right),\\
X_y &= \sin^2\left(\frac{k_y h}{2}\right), \quad \alpha = \frac{\left(V_p^2 - 2V_s^2\right)^2}{4V_p^4}, \quad \beta = \frac{1}{4},
\end{aligned}$$

and

$$\begin{aligned}
\tilde{K}_{11} &= V_p^2 \frac{\tilde{X}_x}{\tilde{D}^2}(1-4\alpha X_y) + V_s^2 X_y(1-\beta\tilde{X}_x),\\
\tilde{K}_{22} &= V_p^2 X_y(1-4\alpha\tilde{X}_x) + V_s^2 \frac{\tilde{X}_x}{\tilde{D}^2}(1-\beta X_y),\\
\tilde{K}_{12} &= \frac{\left(V_p^2 - V_s^2\right)}{\tilde{D}}\sqrt{\tilde{X}_x X_y(1-\tilde{X}_x)(1-X_y)},\\
\tilde{X}_x &= \sin^2\left(\frac{\tilde{k}_x h}{2}\right),\\
\tilde{D} &= \frac{2i\sin\left(\frac{\omega\Delta t}{2}\right) + d_\infty \Delta t\cos\left(\frac{\omega\Delta t}{2}\right)}{2i\sin\left(\frac{\omega\Delta t}{2}\right)}.
\end{aligned}$$

Now the system of equations (A-3) and (A-4) at $i^{\frac{1}{2}} = 0$ gives the value of the reflection coefficients R_{pp}(resp. R_{ss}) and R_{ps}(resp. R_{sp}). We have used the software MAPLE to compute their Taylor expansions with respect to the discretization step h, and we obtained

$$\begin{aligned}
R_{pp} &= \frac{d_\infty - 2d_{\frac{1}{2}}}{4\omega}\left(1-2r_1^2\left(V_p^2+V_s^2\right)\right)\frac{r_0}{V_p}h + O(h^2),\\
R_{ps} &= \frac{d_\infty - 2d_{\frac{1}{2}}}{4\omega}\left(3-2r_1^2\left(V_p^2+V_s^2\right)\right)k_y h + O(h^2),\\
R_{ss} &= \frac{d_\infty - 2d_{\frac{1}{2}}}{4\omega}\left(1-2r_2^2 r_1^2\left(V_p^2+V_s^2\right)\right)\frac{r_0}{V_p}h + O(h^2),\\
R_{sp} &= \frac{d_\infty - 2d_{\frac{1}{2}}}{4\omega}\left(2r_2^2 r_1^2\left(V_p^2+V_s^2\right) - 1 - 2r_2^2\right)k_y h + O(h^2),
\end{aligned} \tag{A-5}$$

with

$$r_0 = \sqrt{\omega^2 - V_p^2 k_y^2}, \quad r_1 = \frac{k_y^2}{\omega^2}, \quad r_2 = \frac{V_s^2}{V_p^2}, \quad r_3 = \frac{1}{r_2}.$$

From relations (A-5), we can remark easily that the best choice for $d_{\frac{1}{2}}$ consists of taking

$$d_{\frac{1}{2}} = \frac{d_\infty}{2}.$$

In that case, the first-order terms in (A-5) disappear and we obtain that the reflection coefficients are approximately proportional to $d_\infty(d_\infty + i\omega)h^2$. Two consequences can be deduced from this result. First, the numerical scheme is consistent with the continuous PML model: The spurious reflection for a given value of d_∞ results only from the dispersion of the numerical scheme. Let us remark that the second-order accuracy is recovered in the h^2 dependency of the reflection coefficients. Then, from a more practical point of view, this dispersion analysis implies that we cannot use a value of d_∞ too large for a given discretization step.

In the case of a finite length layer with a given number of nodes, the layer is characterized by

$$\begin{cases}\left(d_{\frac{1}{2}}, d_{\frac{3}{2}}, \ldots, d_{n_\ell - \frac{1}{2}}\right),\\ \left(d_1, d_2, \ldots, d_{n_\ell}\right),\end{cases}$$

We then are led to find a trade-off between choosing the $d_{i+\frac{1}{2}}$s too small (which would imply a strong reflection caused by the Dirichlet boundary condition) or too large (which would imply spurious reflections caused by the dispersion). A partial answer to this problem is to use a smooth profile for $d(x)$, $(d_{i+\frac{1}{2}} = d(h(i+\frac{1}{2}))$, as is done in the classical layers models (Israeli and Orszag, 1981). An alternative is to determine the best coefficients for $d(x)$ by minimizing the numerical reflection coefficients, as is done in Collino and Monk (1998) for the Helmholtz equation.